

Landslides (2025) 22:17–29
 DOI 10.1007/s10346-024-02335-4
 Received: 14 November 2023
 Accepted: 31 July 2024
 Published online: 30 August 2024
 © The Author(s) 2024

Matteo Roverato  · Lucia Capra



From mixed to hybrid facies volcanic debris avalanche at Colima Volcano: sedimentology and numerical modeling as evidence of transport and emplacement mechanisms

Abstract Numerous partial collapses of Colima Volcano have occurred in its history, accompanied by the emplacement of volcanic debris avalanche deposits (VDADs). The collapse that generated the Tonila VDAD (T-VDAD; $\sim 1 \text{ km}^3$; $\sim 15 \text{ Ka}$ cal. BP) occurred during “wet” paleoclimatic conditions in a high humidity environment, and water within the volcanic edifice, which played a significant role in the volcano’s instability and avalanche transport. This study aims to provide new data on the processes involved in the transport and emplacement mechanisms of debris avalanches based on a detailed granulometric and microtextural characterization and numerical modeling. In general, T-VDAD exhibited massive dynamic behavior during its transport, without segregation process, although some variation of the grains-size occurs from proximal to distal reaches from the source. At microscopic level, evidence suggests particle–particle interactions of rapid, high-energy, high velocity collisional nature, promoting comminution, which increases the fines content with distance. The general high content of fine material into the T-VDAD, combined with a significant water content within the mass before the collapse, due to partial edifice saturation, may have contributed to enhance its mobility. The T-VDAD mobility is here tested with the Titan2d numerical model; results show important paleo-topography implications and that the Coulomb frictional model with basal friction angles similar to previously tested cases best fits the areal propagation of the T-VDAD, confirming that, despite the fluid content that enhanced downslope transformation, the flow still behaved as a homogeneous and incompressible continuum with energy dissipation concentrated within its base.

Keywords Volcanic debris avalanche · Volcano collapse · Colima Volcano · Sedimentology · Numerical modeling · TITAN2D

Introduction

The growth of active volcanoes is often characterized by episodes of partial collapse of their flanks and consequently the formation of volcanic debris avalanches deposits (VDADs). Recently, Dufresne et al. (2021) proposed a new global database containing 1001 known and inferred VDADs (mainly larger than 0.1 km^3) from 594 volcanoes in 52 countries; these numbers are expected to grow. The vast majority of these are Quaternary in age, but VDADs have been identified as far back as the Precambrian (Trofimovs et al. 2004; Roverato 2016). The conditioning and triggering mechanisms of failure are various and complex. Endogenous or exogenous conditionants, such as over-steepened slopes, magma intrusions, hydrothermal

activity, climate fluctuations, deformation of the basement, and faulting, can create the conditions for volcano collapse. Once a volcano reaches its critical point, a mechanism, an earthquake for example, is necessary to trigger the failure event (Siebert et al. 1987; Roverato et al. 2021). Volcano edifice flank collapses are accompanied by the formation of volcanic debris avalanches (VDAs), which are commonly considered as granular flows that move under the force of gravity on the volcano’s slopes. There is an extensive bibliography (Palmer et al. 1991; Glicken 1996; Clavero et al. 2002; Siebert et al. 2004; Bernard et al. 2008; Bernard et al. 2009; Zernack et al. 2010; Roverato et al. 2011; Paguican et al. 2014; Roverato et al. 2018, Norini et al. 2020 among others) that clearly establishes the textural characteristics of these deposits, such as the jigsaw texture of their blocks and the surface morphology of the deposits, characterized by mounds several tens or even hundreds of meters high, which, along with the presence of a horseshoe-shaped scar structure on the volcano, represent the typical features for interpreting the occurrence of a lateral collapse. However, the transport and emplacement mechanism of these debris avalanches is still a matter of debate, as to date, there is no universal model that describes those processes. Recent works have tried to shed light on this topic (e.g., Roverato et al. 2015; Paguican et al. 2021; Procter et al. 2021; Makris et al. 2023a, 2023b) although there is still controversy over the mechanisms that act within the granular mass and how these affect its mobility. This paper aims to provide evidence of the different mechanisms that act inside a moving debris avalanche and how these can contribute to its mobility. In particular, data from a debris avalanche that originated in the Late Pleistocene in the Colima Volcano, T-VDAD, previously described in terms of its origin, stratigraphy and distribution by Roverato et al. (2011), are here presented. A detailed granulometric characterization, microtextural study (using scanning electron microscopy), and the flow numerical model of T-VDAD are used here as a key tool to help understand the dynamics that occurred during the transport and emplacement of this large-scale granular flow.

Colima Volcano

Colima Volcano is one of the most active volcanoes in North America and is part of the Colima Volcanic Complex (CVC). The CVC is a group of andesitic volcanoes located in the western sector of the Trans-Mexican Volcanic Belt (TMVB), a continental volcanic arc that extends across central Mexico. The TMVB is the product of the subduction of the Cocos and Rivera plates beneath the North American Plate (Ponce et al. 1992; Pardo and Suarez 1993). This

magmatic arc has an approximate length of 1000 km and variable width ranging from 80 to 230 km, with a preferential east–west orientation in its central and eastern portion. However, in its western part, it shows a northwest-southeast orientation and is related to the opening of the Gulf of California (Gómez-Tuena et al. 2007). The CVC is located in the Colima graben, which has a northeast-southwest orientation and separates the Jalisco Block from the North American Plate to the west and the Michoacán Block to the east (Ferrari et al., 1994, Bandy et al. 2005). The CVC is composed of three andesitic volcanic edifices: Cántaro, Nevado de Colima, and Colima Volcano. These three eruptive centers are aligned north–south and are likely controlled by a local fault system which may have influenced the migration of volcanism to the south and the instability of the volcanic complex (Norini et al. 2010), which

has experienced several volcanic collapses with the emplacement of multiple VDADs (Luhr and Prestegaaard 1988; Stoores and Sheridan 1992; Komorowski et al. 1997; Capra and Macias 2002; Cortés et al. 2010, Roverato et al. 2011; Cortés et al. 2019; Capra et al. 2021). Colima Volcano (Fig. 1), also known as *Volcán de Fuego*, is the youngest edifice of the CVC and consists of the recent and active cone, which was built inside the Paleofuego scarp, a relict structure of an ancient sector collapse. Although previous works provided different ages for the formation of the Paleofuego collapse, thought in any case not to be older than 10 Ka (Luhr and Prestegaaard 1988; Robin et al. 1987), Roverato et al. (2011) asserted that the Paleofuego collapse was indeed older than the T-VDAD event (> 15 ka) and that the deposit here studied originated from a discrete collapse of the recent Colima Volcano.

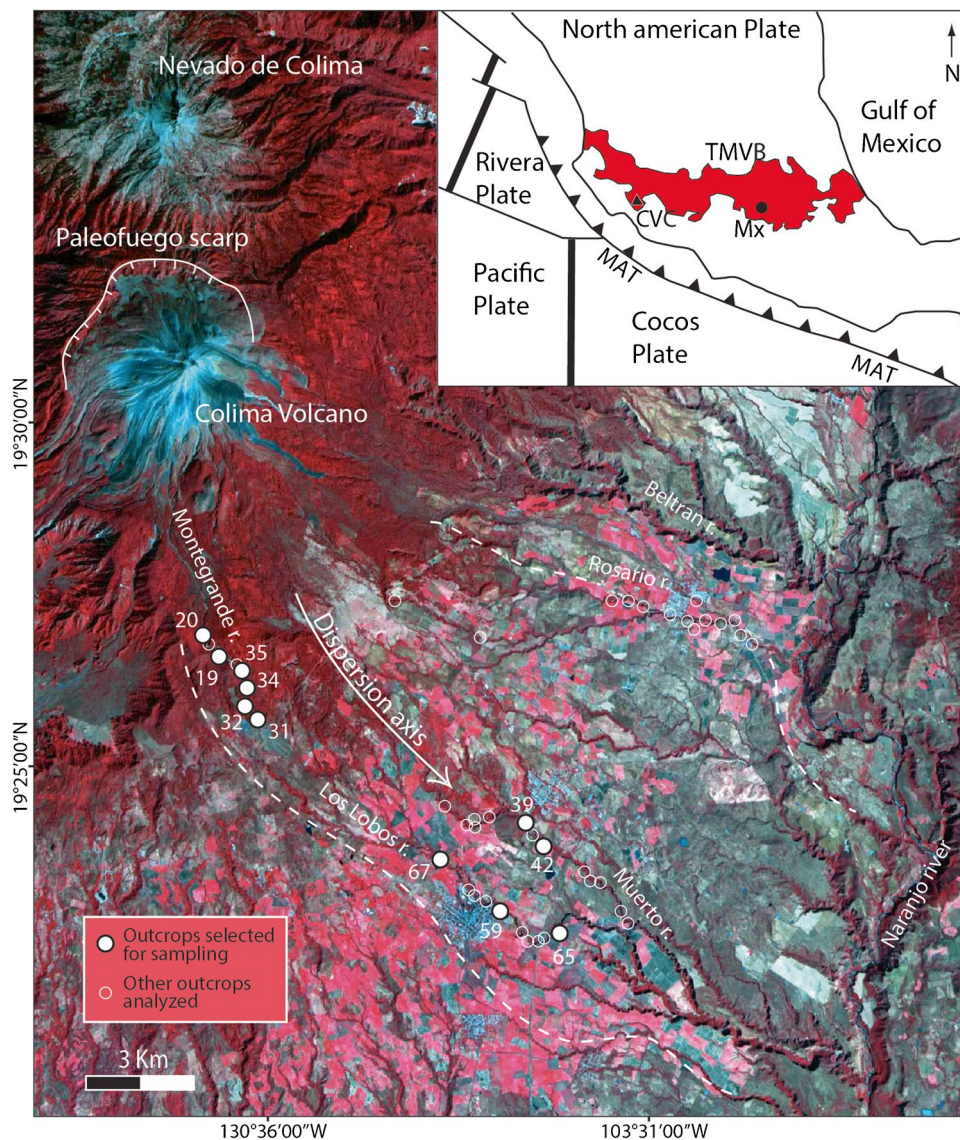


Fig. 1 Location map of the Colima volcanic complex (CVC) in the regional setting of the Trans Mexican Volcanic Belt (TMVB); MAT: Middle American Trench; Mx: Mexico City (inset top right). The aster image shows the location of the analyzed outcrops (both white dots and circles) useful for lithofacies characterization, thickness of the deposit and stratigraphic correlation, and the sampled outcrops Pcr# (white dots) for sedimentology studies. Dashed line shows the inferred dispersion of the Tonila volcanic debris avalanche deposit (VDAD)

Tonila VDAD

The stratigraphy of T-VDAD was described in detail by Roverato et al. (2011). This deposit covers an area of approximately 200 km² and is delimited by the Naranjo River to the southeast and the Beltran Ravine to the northeast (Fig. 1). Its volume is approximately 1 km³, and radiocarbon dating of organic materials has yielded ages of ~15 ka cal. BP.

Tonila collapse occurred during the final phase of the last glacial maximum (18–15 ka cal. BP), a period characterized by high humidity and the possible presence of a snow/ice cap on the volcano's summit, along with significant water circulation within the edifice (Roverato et al. 2011; Capra et al. 2013). The Tonila event was strongly influenced by paleoclimatic conditions, which played a significant role in the instability of the volcanic edifice and in the mechanisms of transport and emplacement of the avalanche. T-VDAD exhibits abundant clasts showing jigsaw-like structures, poor mixing often leading to the preservation of original stratigraphy and abrupt facies changes along the deposit, especially in proximal reaches (<8 km from the source). These changes are more evident, mainly in those portions that show color stains due to different degrees of hydrothermal alteration (Fig. 2a). However, in marginal and distal reaches (>15 km), there is a noticeable change in texture. It is characterized by an abundant, more homogeneous, and partially cemented sandy matrix (Fig. 2b) often surrounding more heterogeneous portions. This facies has been defined as hybrid (Capra et al. 2002; Roverato et al. 2011; Bernard et al. 2021), as it shows transitional characteristics between a debris avalanche and a debris flow, which is related to the presence of abundant water in the mass before its remobilization. The deposit is generally characterized by the abundance of clasts smaller than 256 mm and abundant matrix (matrix facies—Mf, following Roverato et al. 2011). Furthermore, the Tonila event was characterized by a post-collapse eruption, as evidenced by the presence of pyroclastic deposits directly in contact with the avalanche. Textural characteristics of the pyroclastic material indicates hydromagmatic features (see Roverato et al. 2013), demonstrating, once again, a high fluid circulation within the volcano edifice during the failure event.

Methodology

During our field campaigns, several outcrops were analyzed (Fig. 1), with prior detailed facies mapping necessary due to the high sedimentological variability of the deposit. In proximal reaches, where the deposit is chaotic and unmixed, displaying different lithological “domains” (terminology of Palmer et al. 1991), we sampled the interclast matrix, which describes the fine sediment that forms an embracing interconnected body of particles that support or fill gaps between clasts (terminology of Roverato et al. 2015). In medial/distal reaches, when the deposit becomes more homogeneous, samples are from the whole rock. A total of 11 samples from 11 outcrops (Pcr#—Fig. 1) were collected (in bags of ~1 kg each) to investigate the possible longitudinal evolution of the deposit along a given dispersion axis (Fig. 1). For the coarser portion (>4φ), photographs (outcrop surface area >1 m²) were taken for image processing. Samples were processed for the granulometric analyses by three different methods: the –9φ to –4φ (512 to 16 mm) fraction was analyzed by image analysis following the method proposed by Sarocchi et al. (2005); the –3φ to 4φ (8 mm to 63 μm) fraction was measured by dry sieving at 1φ intervals; finally, a laser particle sizer

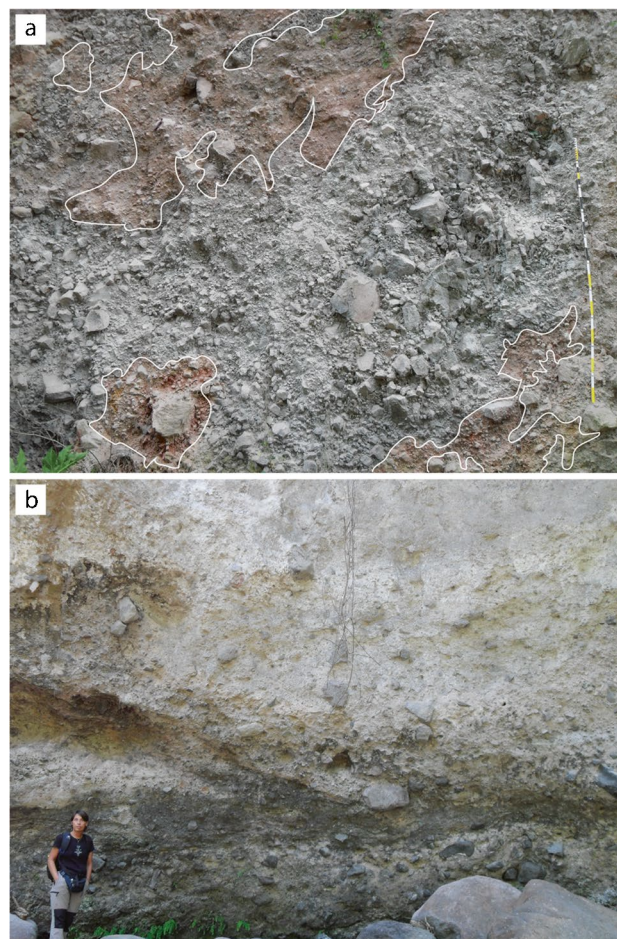


Fig. 2 Two photographs of the Tonila VDAD showing the facies variability between the proximal (a) and the medial/distal (b) reaches. White lines in photograph a highlight the different lithologies

(Fritsch–Analysette 20 photosedimentograph) was used to determine the 4φ to 9φ (63 to 2 μm) classes with a 1φ interval.

Standard Folk statistical parameters (Mean—Mz, standard deviation or sorting—σ, and skewness—Sk) were calculated using KWare SFT program (version 2.19.0168* from Ken Wohletz, 31 July 2007). Grain size fractions are chosen because comparison of their distribution and abundance can allow the evaluation of the comminution processes and any preferential comminution of size classes. The sorting coefficient (σ) describes the range in size required to encompass a given majority of the population around the mean. A low sorting coefficient thus describes a population with little spread around the mean (i.e., good sorting). A higher sorting coefficient indicates that the population is spread over a larger range of sizes (i.e., poor sorting). Skewness (Sk) measures the degree to which the population approaches symmetry. Positive skewness describes populations with large proportions of fine material (fine-skewed) and a tail in the coarser range of sizes, and negative skewness the opposite (coarse-skewed). A skewness of zero would describe a symmetrical distribution.

Sand particle surface features were examined using a JEOL-35C scanning electron microscope (SEM) equipped with a TRACTOR

NORTHERN energy-dispersive detector at 15 kV and a 20-s acquisition at CGEO-UNAM (Queretaro, Mexico). We examined 10 samples collected on 7 sites (Pcr 20/35/31/32/67/59/65). Each sample consisted of 10 to 15 particles (both lithics and pyroxene crystals) from 2 mm to 500 μm in size. The samples were taped on top of aluminum cylinders and carbon coated.

The Titan2D numerical model (Patra et al. 2005) has been widely used to simulate dry granular flows such as pyroclastic density currents (Patra et al. 2020 and references herein) and volcanic debris avalanches (i.e., Cortes et al. 2010). The TITAN2D code employs depth-averaged shallow water equations for the conservation of mass and momentum. The 4.1.1 code version offers the Mohr–Coulomb model for dry avalanches and the Pitman and Le (2005) two phases, for a continuous mixture of fluid and solids. Mohr–Coulomb model is a simple stress-dependent model with friction terms for the interactions between the granular medium and the basal surface. The two-phase model is formulated to account for the dynamics of both solid particles (granules) and the interstitial fluid (typically air or water) within the flowing mass, taking into account the buoyancy effect coupled with pore fluid pressure. The theory of the models is extensively described by Patra et al. (2020) and Neglia et al. (2021). Here, both models are used to better understand how the wet condition of the edifice prior to the collapse can have enhanced the T-VDAD mobility. To perform the simulations, the main input parameters are the volume of the sliding mass, the basal friction angle, and, in the case of the two-phase model, the volumetric proportion between solid and fluid. The sliding mass is designed with an ellipsoidal basal shape, where the main axis is oriented toward the main collapse direction based on the deposit distribution, in this case in a range of 35° SE to 60° SE. Simulations are performed on a Digital Elevation Model with a 10-m pixel resolution (Alos-Palsar, 2011). The output of the simulation is a raster representing the maximum flow thickness at each pixel. Simple raster algebraic operations are used to combine all simulations to obtain a final distribution map that includes all pixels that are inundated based on the different input parameters used (Table 3). One of the main limitations of the modeling presented here is that the current topography is far from the paleomorphology at the moment of the volcanic collapse. To limit this effect, the main cone was modified recreating the horseshoe scar by removing a 1 km³ mass that is in the range of the volume estimated for the T-VDAD (Roverato et al. 2011) and eliminating the Los Hijos domes (see the “Flow numerical modeling” section) as, based on the first result, they produce a flow deviation not observed in the field. The depositional area was not modified due to several uncertainties about the topographic base of the T-VDAD. Finally, the “dry” (Mohr–Coulomb) and “wet” (Pitman and Le) models that the code offers (Patra et al. 2005; Neglia et al. 2021) are here used to define the conditions that could have promoted the flow mobility and the observed runout. Raster operations were performed using a GIS application.

Granulometric characterization

The charts in Fig. 3 display the granulometric distribution of the investigated deposit, from the selected proximal to distal outcrops (see Fig. 1). In general, granulometric distributions exhibit a polymodal pattern, with some samples exhibiting more marked modes between -5ϕ and -3ϕ for coarser fractions and $3\phi/4\phi$ for finer fractions; a few others show modes in the silt range between 5ϕ and

7ϕ . Overall T-VDAD is poorly sorted, with significant lateral facies variations. For instance, the charts Pcr35 and 32 (Fig. 3) exhibit significant similarity but are quite different from sample Pcr34, even though all the three outcrops are relatively close.

T-VDAD apparently presents a granulometric variation with distance. For example, considering the two extremes, Pcr20 (most proximal outcrop—6.3 km) and Pcr65 (most distal outcrop—16.2 km), a change in granulometry (decrease in coarse particles and increase in sand and fines) with distance is noticeable (Table 1). Pcr65 shows a notable increase in values for each fraction between 0ϕ and 3ϕ , along with a considerable increase in the silt–clay fractions (5ϕ – 9ϕ). T-VDAD has gravel content ranging from 20 to 75% by weight, with a higher concentration between 20 and 60% and an average value of 48% (Table 1). The sand content ranges from 22 to 67% by weight, with higher concentration between 30 and 50 with an average value of 45%. The matrix content (Table 1) is quite abundant in T-VDAD and varies from 24 to 79% by weight, with an average value of 52%. The content of fines (silt + clay) has a fairly high percentage, ranging from a minimum of 2 to a maximum of 17% by weight, with a more abundant concentration between 5 and 9% and an average value of 7%, while the clay content is low, with a maximum value around 0.7% and an average value of 0.4% by weight (Table 1).

Table 2 shows the statistical parameters (mean, standard deviation, skewness—Folk and Ward 1957) organized from proximal to distal outcrops. The Mean (Mz) remains mostly negative, although it increases with distance. In Fig. 4, the diagram of distance from the source vs. Mean grain size (Mz), displays the general increase in fine particles with distance. Sorting (σ) varies between 2.62 and 4.19 reflecting very to extremely poor sorting with no changes with distance (Fig. 5a) and Skewness (Sk) exhibits a slight decrease with increasing of distance (Fig. 5b). Thus, initially, coarser material composes the majority of the mass with the finer particles generating a “tail” in the grain size distribution. During transportation, accompanied by comminution, fines become the majority of the grain size distribution; however, a significant coarse component is preserved as a “tail.”

Microscopic textures

The microscopic analysis show textures consisting of different types of fractures, parallel grooves, and scratches giving place to different intensity, lips, percussion marks, staircase geometry, and broken crystals. The clasts generally exhibit heterogeneous morphologies from elongated to spherical, with angular or rounded portions with perfectly rounded edges. Fractures are generally present in both lithic fragments (Fig. 6a–c) and crystals (Fig. 6b, d). It is common to observe fractures in lithics propagating both in the clast matrix and in the crystals within the clast (Fig. 6b). In contrast, fractures in crystals generally do not propagate into the clast matrix. It is quite common to observe truncated crystals (Fig. 6e) and/or broken ones, as well as features defined as “stair-step” or “staircase” geometry due to tearing apart (Fig. 6f–h) (Komorowski et al. 1991; Caballero and Capra 2011). Figure 6i shows an irregular fracture with a small “pull-apart” structure that indicates the kinematics of the movement of the two portions of the grain. Impact marks are abundant, as shown in Fig. 6l with a sequence of consecutive impacts, in contrast with a wider impact mark on a crystal shown in Fig. 6m. Other characteristic features include scratches

Tonila VDAD

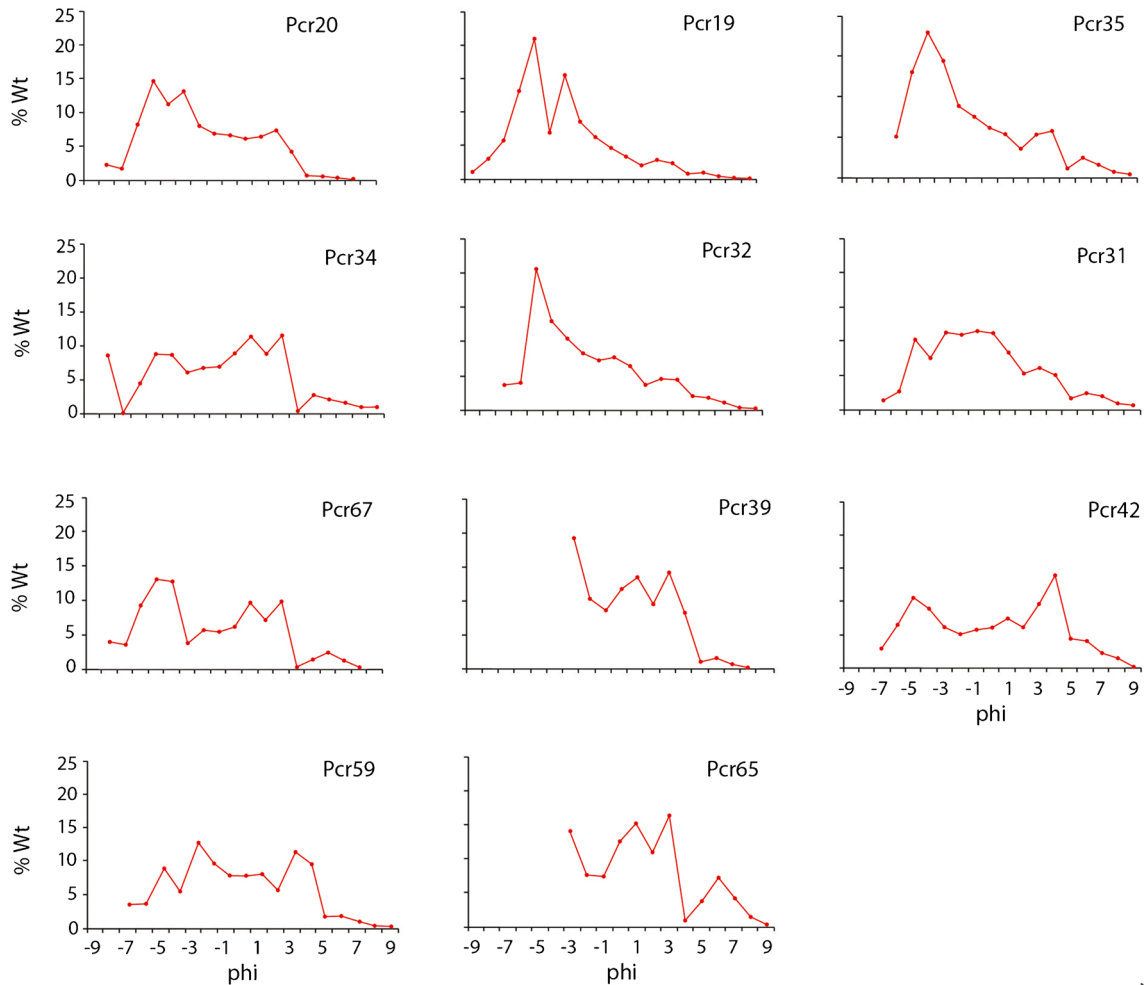


Fig. 3 Grain-size diagrams for the Tonila VDAD with distance from source

and grooves even if less common. Parallel grooves can be observed on a pyroxene crystal in Fig. 6n.

Flow numerical modeling

Based on the volume estimation of the T-VDAD (~1 km³, Roverato et al. 2011) and its extent (Fig. 1), simulations were executed using the “dry” (Coulomb) and “wet” (Pitman and Le) models (Table 3). For the frictional rheology, basal friction angles between 6 and 9° were used, in the range of those used to reproduce debris avalanches in other volcanoes (Le Friant et al. 2003; Cortes et al., 2010; Borselli et al. 2011; Sosio et al. 2012). The initial pile was accommodated in the reconstructed horseshoe scar with a volume of ~0.8 km³, estimated from the total volume of the T-VDAD of 1 km³, minus 20%, which could be related to expansion of the material during flow (Glicken 1996). The first results show that the collapsing mass was strongly affected by the Los Hijos domes, a topographic high on the slope of the main cone (Fig. 7a), by deviating a portion of the flow toward the SW, an area where the deposit has not been observed, and limiting flow inundation along the Montegrande

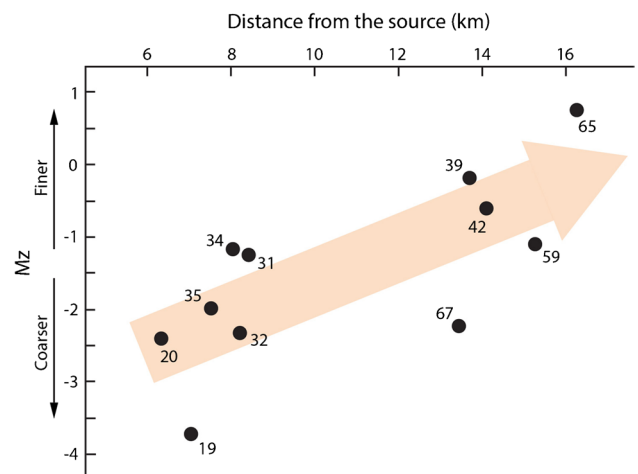
ravine where the deposit show thickness up to 15 m (Roverato et al. 2011). Consequently, the domes were digitally removed from the DEM, obtaining results (with the same input parameters) that best reproduced the area distribution of the T-VDAD (Fig. 7b). Flow overspill on the SW is still observable because of the uncertainty in defining the landslide scar, but with a much more reduced effect due to the removal of Los Hijos domes from the simulation. The final distribution map (Fig. 8) was obtained considering the maximum flow thickness at each 10-m pixel based on all simulations with variable parameters as indicated in Table 3 (Fig. I in supplementary material). As previously mentioned, the depositional area corresponds to the present topography, so the main ravines that are now eroded in the T-VDAD did not exist at the moment of the event, including the Beltran ravine where the simulated flow channels into it and reaches the Naranjo river (Fig. 8). For the two-phase simulations, the same pile volume was used, with basal friction angle between 24 and 28° (Neglia et al. 2021) and solid volume fraction between 0.8 and 0.9. None of the simulations were able to reproduce the observed areal distribution, with higher basal

Table 1 Gravel-sand-fines content (wt%) for samples of the Tonila VDAD organized from proximal to distal from the source

Sample	Km from source	Gravel (-8ϕ a -2ϕ)	Sand (-1ϕ a 4ϕ)	Silt (5ϕ a 8ϕ)	Clay ($\geq 9\phi$)	Fines (L + Arc)	Matrix ($-1/9\phi$)
Pcr20	6.3	59.82	38.15	1.93	0.1	2.03	40.18
Pcr19	7	75.35	21.92	2.57	0.16	2.73	24.65
Pcr35	7.5	59.59	33.95	6.0	0.45	6.45	40.4
Pcr34	8	43.46	48.03	7.5	1.0	8.5	56.53
Pcr32	8.2	60.1	34.22	5.42	0.27	5.69	39.91
Pcr31	8.3	44.34	47.79	7.21	0.72	7.93	55.72
Pcr67	13.4	53.66	38.85	6.28	0.21	6.49	45.34
Pcr39	13.7	29.87	66.5	3.56	0.06	3.62	70.12
Pcr42	14.1	39.59	48.20	12.1	0.2	12.3	60.5
Pc59	15.3	44.01	50.34	5.27	0.38	5.65	55.99
Pcr65	16.2	21.04	61.55	16.7	0.71	17.41	78.96
Mean value		48.3	44.5	6.8	0.4	7.2	51.7

Table 2 Statistical parameters (Mz, σ , and Sk) for the Tonila VDAD organized from proximal to distal from the source

Samples	Mean (Mz)	Sorting (σ)	Skewness (Sk)
Pcr20	-2.41	3.4	0.28
Pcr19	-3.74	3.17	0.27
Pcr35	-1.97	3.55	0.45
Pcr34	-1.19	4.19	-0.11
Pcr32	-2.37	3.48	0.35
Pcr31	-1.26	3.55	0.16
Pcr67	-2.22	3.99	0.17
Pcr39	-0.17	2.62	-0.02
Pcr42	-0.61	4.15	-0.09
Pcr59	-1.11	3.65	0.03
Pcr65	0.78	3.28	0.1

**Fig. 4** Diagram showing the trendline (trend orange arrow) of mean grain size (Mz) vs. distance from the source suggesting a general increase in fine particles with distance; the outcrops follow the axis of the dispersal directions shown in Fig. 1

friction angles forcing the flow to stop in the proximal reaches, while lower angles produced high-velocity flows that run straight in the direction of the collapse (see Fig. II in supplementary material).

Discussion

The Tonila VDAD presents as a “dry” deposit in proximal reaches showing characteristics of poor mixing (e.g., Fig. 2a), preservation of original stratigraphy, abrupt facies variations, with characteristics changing to pervasive and homogeneous matrix facies (hybrid facies) in marginal and distal reaches (e.g., Fig. 2b). This represents

a transformation from granular/frictional-dominated flow regimes to a debris flow-like type due to the water content and the increasing fines content with distance. As the Colima Volcano was water semi-saturated during the Tonila event due to snow/ice melting and high environmental humidity (Roverato et al. 2011; Capra et al. 2013), it appears reasonable that water played a role in the propagation of the avalanche, even though it was not present in quantities that enable it to entirely become the transporting medium and transform to a cohesive debris flow. In fact, despite its apparent availability, water was not uniformly distributed throughout the Colima edifice and consequently not in the Tonila VDAD. Water

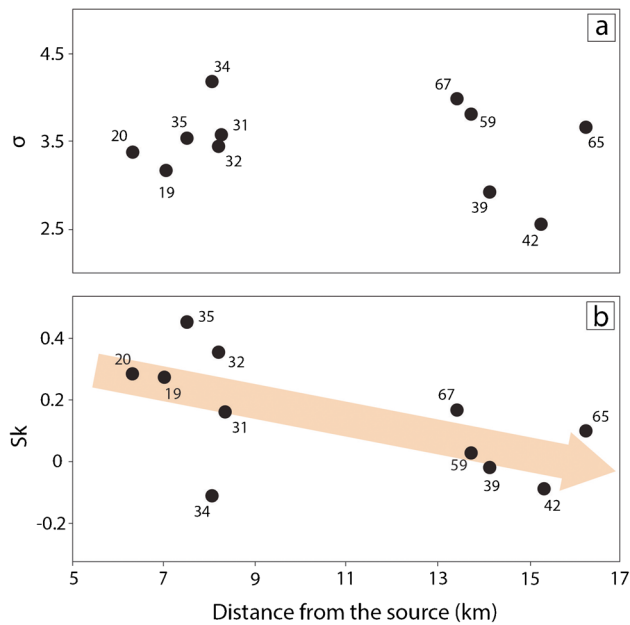


Fig. 5 **a** Sorting (σ) vs. distance from the source diagram illustrating no trends with distance; **b** skewness (Sk) exhibits a slight decrease with increasing distance (trend orange arrow)

enhanced flow mobility and achieved saturation levels probably only in localized positions for short periods. It appears then that water, although is an important factor that influenced the propagation of Tonila VDAD, was not the only factor acting during the avalanche mobility. We believe, therefore, that the effects of inertial collision of solid fragments played a very significant role rather than only water effects. It would suggest that particle–particle interactions power the mobility of volcanic debris avalanches, as also recently demonstrated by Makris et al. (2020). The Tonila VDAD is characterized by a high matrix content, and this study indicates that the matrix production is primarily an interior-flow process and caused by brecciation/crushing and comminution of the lithologies during transportation. The granulometric analysis of Tonila deposit shows a general increasing of Mean grain size (Mz) with distance (Fig. 4), which could be also explained by the presence of water that may have played an important role in segregation processes with the progressive deposition of larger fragments with distance. However, progressive fragmentation and comminution processes produced a gradual clast-size reduction with distance from the source and gravel proportion decreased as the proportion of sand-sized particles increased; therefore, an exchange between the gravel and sand component is noticeable for T-VDAD (Table 1). The generation of finer material is thought to be responsible for the increased matrix with distance, and the average clast size is progressively reduced due to the gradual abrasion and fracturing of clasts in the agitated matrix (Perinotto et al. 2015; Paguican et al. 2021; Makris et al. 2023a). The sorting (σ) remained largely unaffected in the very poorly sorted range (Fig. 5a) while skewness decreased with the increased of distance (Fig. 5b). The decreasing trend of Sk suggests that a substantial amount of the coarse particles is preserved even though progressive comminution reduces the size of the initially

dominant coarse gravel. It appears that a preferential comminution of finer particles prevails because fragmentation of the larger fractions requires collision with grains of equal or larger size implying more energy dissipation (e.g., Davies and McSaveney 2009). This is also confirmed by the charts in Fig. 3 that show how a coarse mode was preserved as a second mode developed in the sand size range with the progressive increase in fines with distance. In other words, coarser particles immersed into the moving mass fragment less than the finer during transportation in agreement with Makris et al. (2020). It could justify the very poor sorting of T-VDAD as confirmed by the high values of σ along the entire deposit. The SEM analyses provides evidences of the surface textural characteristics of the Tonila deposit sand-size particles, suggesting that the forces involved during T-VDAD transport are mainly of collisional-type between particles. The collision between two grains is punctual, rapid, high-energy, and high-speed, resulting in deep impact marks, partial fractures of the particles/crystals, or through-fractures as also observed by Caballero et al. (2014). These latter authors show that sand particles comminute because of these high-impact collisions, contributing to the increase the finer portion of the mass, while coarse particles do not break completely, developing smaller fractures that provide minor “flakes,” which contribute along with the finer particles to the overall population (Fig. 9). This increase of fine material further limits the interaction between larger particles. In contrast, if collisions are repeated and of lower energy, they can leave several lower-intensity impact marks in the same area of a particle without necessarily breaking or fracturing the particle. This fact can be explained by considering that some particles did not have enough space to move and thus interacted by vibrating. Shear stress acting in a moving avalanche is mainly reflected in the scratches and grooves on the particles, which also indicate different interaction intensities between them, defined by the depth of the marks. Overall, the microscopic evidence suggests a predominant normal grain-grain interaction during transport in a high-energy setting, while evidence of shear stresses is much less represented in our grain-size data.

Most volcanoes that experienced collapse consist of lava flows alternating with weaker and/or unconsolidated deposits that may be locally water-saturated and/or hydrothermally altered. These variabilities are difficult to consider during numerical simulations, and available models are based on a single rheological model. As previously observed by Sosio et al. (2012), the bulk friction angles required to simulate the basal resistance in a frictional rheology model are considerably smaller than the real mechanical properties of dry material (i.e., 38–44° estimated for rocks involved in the Mt. St. Helens collapse—Voight et al., 1983) considering that internal water and/or air pore pressure in some portion of the sliding mass can play an important role in reducing the material resistance or the presence of a lubricating saturated basal layer (i.e., Parinacota volcano, Chile; Clavero et al. 2002). Titan2d simulations that best fit the observed areal extent of the T-VDAD were obtained with the frictional rheology, with angles between 6 and 10°, in the range of values used for the 1980 Mt. St. Helens VDAD (Sosio et al. 2012). The “wet” two-phase model failed to reproduce the observed deposit distribution, confirming that the flow was not fully saturated. Downflow textural changes of the T-VDAD show that only the partially saturated portions of the flow had larger

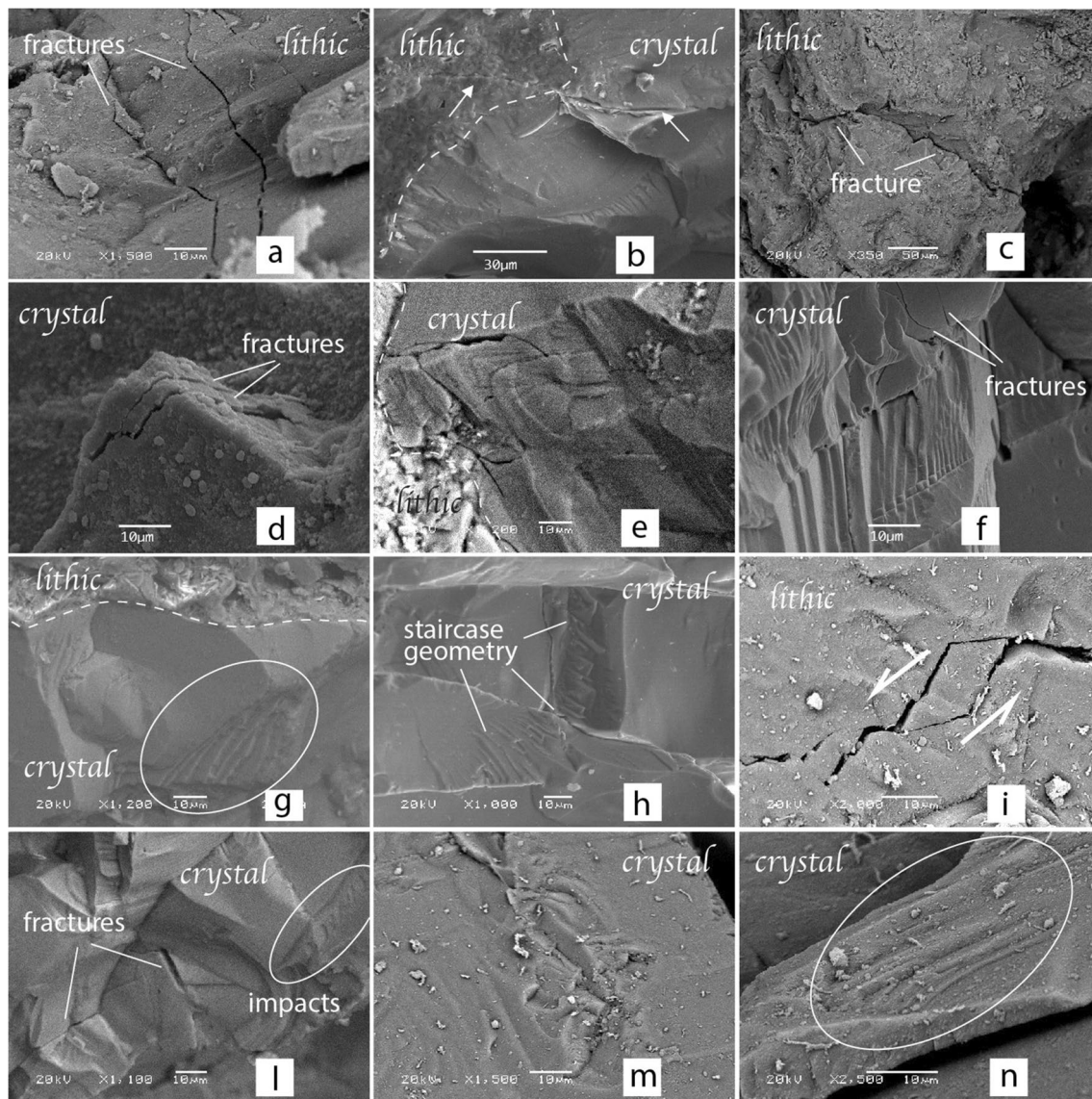


Fig. 6 Scanning electron microscope images of the Tonila VDAD lithics and crystals, showing different features found in the particles analyzed. **a** Fractures in lithic clast; **b** fracture propagating both in the lithic clast and in the crystals within the lithic clast (white arrows); **c** fracture in lithic clast; **d** fractures in pyroxene crystal; **e** truncated crystal; **f** staircase geometry and fractures; **g** stair-step geometry (white circle); **h** staircase geometry; **i** “pull-apart” fracture; **l** fractures and small impact marks (white circle); **m** bigger impact mark; **n** parallel grooves on a pyroxene crystal (white circle). Photographs **e**, **i**, **h**, **m** are from Roverato and Capra (2013)

runouts, so only a mixed flow rheology model could be able to take into account this complex rheological behavior. Variable topography has a minor influence on modeling of the area extent of large-volume VDAs as long as the flow propagates in the absence of a strong topographical barrier. As here observed, the area extent of the T-VDAD is better reproduced only when the Los Hijos domes, which represent a topographic barrier of up to 200 m, are removed from the topography. The age of this dome structure was not previously defined, but, based on the results of the simulations, they are possibly younger than the T-VDAD event, so less than 15 ka. Other discrepancies between simulated flow and the inferred T-VDAD distribution, especially in the northern and distal limits, are the effect of simulating on the present topography where morphology

results from the emplacement of at least five younger VDADs (at 9370 years, 4280 years, 7040 years, 3600 years, 2550 years; Robin et al. 1987; Luhr and Prestegard 1988; Komorowski et al. 1997; Cortés et al. 2010, 2019). It is thus impossible to reconstruct the paleo topography prior to the T-VDAD, in contrast to successful modeling for VDADs where the post-VDAD surface is completely exposed (e.g., Socompa volcano, Chile; Kelfoun and Druitt 2005).

Conclusions

The sedimentological evidence presented in this study suggests that the mechanisms acting during the transport and emplacement of volcanic debris avalanches do not operate uniformly within them. The textural complexity of these bodies, the high

Table 3 Parameters used for Titan2d simulations. Only more representative results are here reported

Number	Coulomb	Two phases	Basal friction angle	Collapse direction (from E to S)	Volume fraction
171 (<i>DEM post Hijos</i>)	x		6°	–30°	
447	x		6°	–30°	
347	x		7°	–45°	
712	x		9°	–45°	
599	x		7°	–60°	
674	x		8°	–60°	
681	x		9°	–60°	
513	x		7°	–35°	
086	x		8°	–35°	
044	x		9°	–35°	
055		x	28°	–45°	0.9
099		x	26°	–45°	0.9

For all simulations, pile dimension is 600 (H), 1200 (L), and 700 (w), and internal friction angle is 37°

topographical variability of different volcanic environments, the various triggering mechanisms of collapse events, and the influence of exogenous factors belonging to different climatic regions force us to consider each avalanche event as unique, responding to its specific transport and emplacement mechanisms. Microscopic analyses here presented possibly indicate that during the transport of the Tonila VDAD, the predominant mechanism involved in the transport was high-energy normal impact-type interactions, with evidence of shear stresses (scratches and grooves) being much less significant in comparison. Several deep impact marks, fractures of varying intensity, and partially broken crystals indicate collisional interactions between particles. The comminution of sand-size particles prevails during transport compared to larger fractions, which requires collision with grains of equal or larger size implying more energy dissipation. Thus, comminution and disaggregation increase the amount of matrix in the moving mass, possibly enhancing its mobility. Furthermore, due to the climate condition during the Tonila event,

the presence of water was a factor influencing and controlling its transport. The water content in the moving mass contributed to increase mobility and facilitated lateral transformation of facies from “typical” features of volcanic debris avalanche to a more homogeneous matrix defined as hybrid facies with strong erosive power. The T-VDAD mobility tested with the Titan2d numerical model shows important paleo-topography implications, and that the Coulomb frictional model with basal friction angles similar to previously tested cases best fits the areal propagation of the Tonila VDAD. This confirms that, despite the water content that enhanced downflow transformation, the flow still behaved as a homogeneous and incompressible continuum with energy dissipation concentrated within its base. The Tonila VDAD cannot be considered as a homogeneous mass with a viscous or viscoplastic flow regime, such as in debris flows, and neither is it representable by pure dry granular flow where particles-particles interaction predominates, but a combination of both these mechanisms that together favor its long run-out.

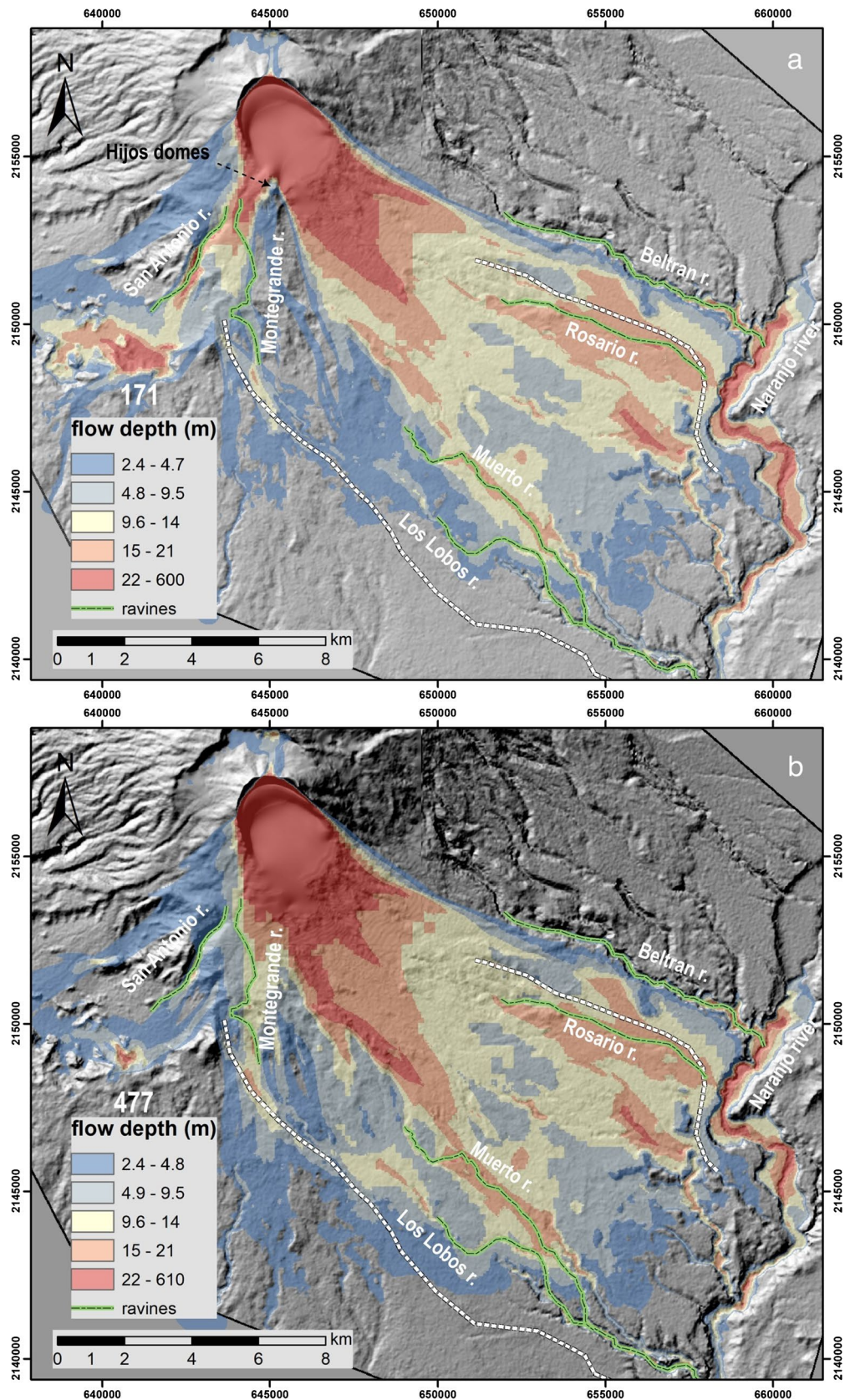


Fig. 7 Results of Titan2D simulations over a topographic relief with (a) and without (b) the Los Hijos dome complex. Note that this topographic barrier is able to strongly control the emplacement of the Tonila VDAD in the south and western sectors. Dashed line shows the inferred dispersion of the Tonila VDAD

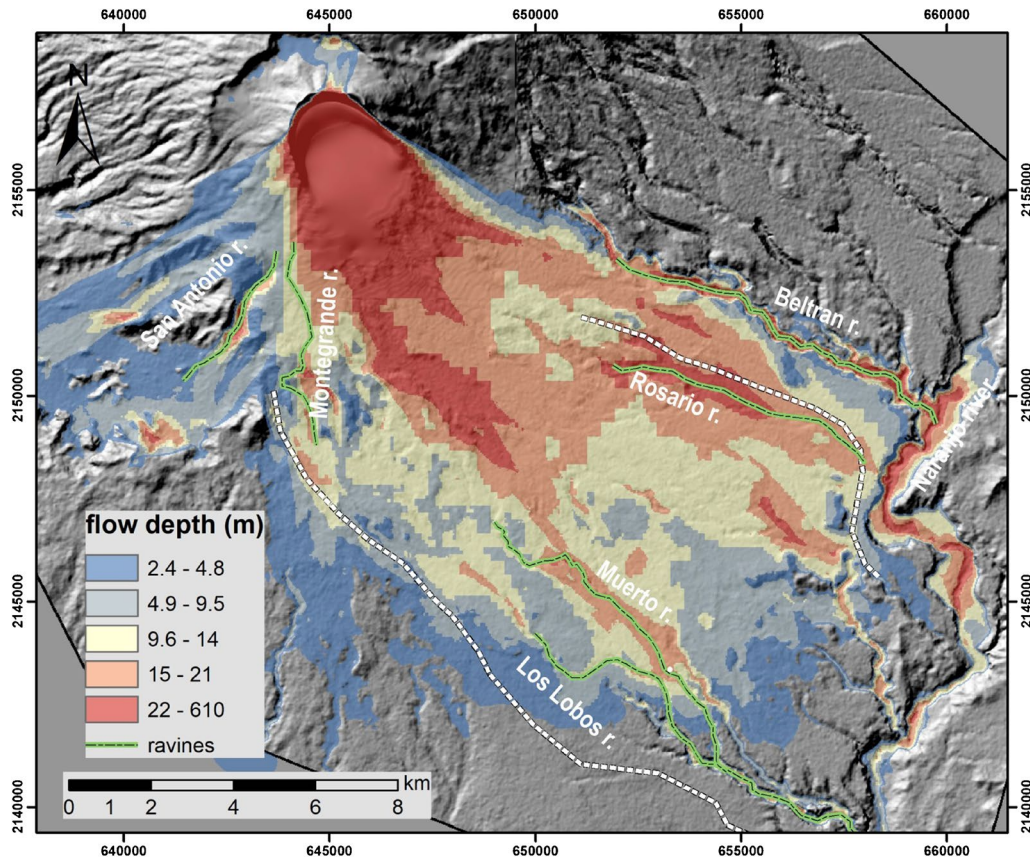


Fig. 8 Final distribution map of the Tonila VDAD reconstructed based on the Titan2D simulations (Table 3 and Fig. II in the supplementary materials). Dashed line shows the inferred dispersion of the Tonila VDAD

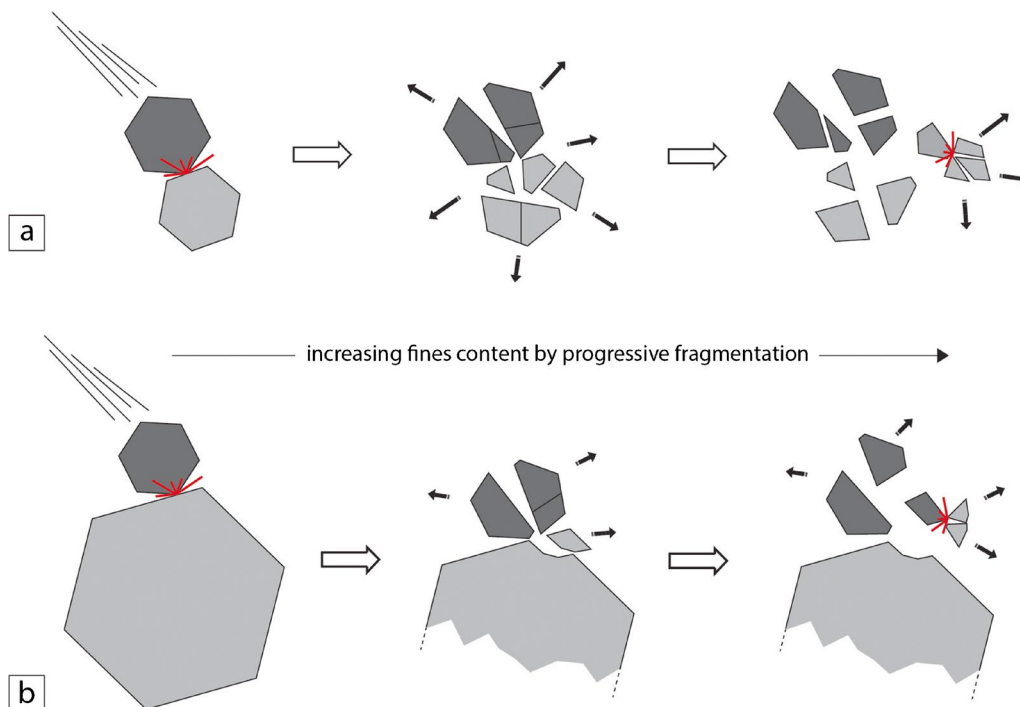


Fig. 9 Sketch representing the impact of two fine sand particles (a); the comminution, due to high-impact collisions, contributes to increase the finer portion of the moving mass. On the other hand, the impact with a coarser particle (b) does not break the latter one but provides minor “flakes,” which contribute to the finer particles in the overall population. It could explain the very poor sorting of the Tonila VDAD as confirmed by the high values of σ along the entire deposit

Acknowledgements

We would like to thank Federico Di Traglia and an anonymous reviewer for their helpful suggestions and corrections, which considerably improved the manuscript.

Funding

Open access funding provided by Alma Mater Studiorum - Università di Bologna within the CRUI-CARE Agreement. This work was supported by the project nos. 46340, 99486 (CONACYT), 14 (SRE-CONACYT), and IN106710 (UNAM).

Data Availability

I declare that the data supporting this study are available upon request from the corresponding author.

Declarations

Conflict of interest The authors declare no competing interests.

Open Access This article is licensed under a Creative Commons Attribution 4.0 International License, which permits use, sharing, adaptation, distribution and reproduction in any medium or format, as long as you give appropriate credit to the original author(s) and the source, provide a link to the Creative Commons licence, and indicate if changes were made. The images or other third party material in this article are included in the article's Creative Commons licence, unless indicated otherwise in a credit line to the material. If material is not included in the article's Creative Commons licence and your intended use is not permitted by statutory regulation or exceeds the permitted use, you will need to obtain permission directly from the copyright holder. To view a copy of this licence, visit <http://creativecommons.org/licenses/by/4.0/>.

References

- Bandy W, Michaud F, Bourgeois J, Calmus T, Dymont J, Mortera-Gutiérrez CA, Ortega-Ramírez J, Pontois B, Royer JY, Sichlerg B, Sosson M, Rebolledo-Vieyra M, Bigot-Cormier F, Díaz-Molina O, Hurtado-Artunduaga AD, Pardo-Castro G, Trouillard-Perrot C (2005) Subsidence and strike-slip tectonism of the upper continental slope off Manzanillo, Mexico. *Tectonophysics* 398:115–140
- Bernard B, van Wyk de Vries B (2009) Distinguishing volcanic debris avalanche deposits from their reworked products: the Perrier sequence (French Massif Central). *Bull Volcanol* 71:1041–1076
- Bernard B, Van Wyk VB, Barba D, Leyrit H, Robin C, Alcaraz S, Samaniego P (2008) The Chinborazo sector collapse and debris avalanche: deposit characteristics as evidence of emplacement mechanisms. *J Volcanol Geoth Res* 176:36–43
- Bernard B, Takarada S, Andrade SD, Dufresne A (2021) Terminology and strategy to describe volcanic landslides and debris avalanches. In: Roverato M, Dufresne A, Procter J (eds) *Volcanic debris avalanches: from collapse to hazard*. Springer book series advances in volcanology 364
- Borselli L, Capra L, Sarocchi D, De la Cruz-Reyna S (2011) Flank collapse scenarios at Volcán de Colima, Mexico: a relative instability analysis. *J Volcanol Geoth Res* 208:51–65
- Caballero L, Capra L (2011) Textural analysis of particles from El Zaguán debris avalanche deposit, Nevado de Toluca volcano, Mexico: Evidence of flow behavior during emplacement. *J Volcanol Geoth Res* 200:75–82
- Caballero L, Sarocchi D, Soto E, Borselli L (2014) Rheological changes induced by clast fragmentation in debris flows. *J Geophys Res Earth Surf* 119:1800–1817
- Capra L, Macías JL (2002) The cohesive Naranjo debris-flow deposit: a dam breakout flow derived from the Pleistocene debris-avalanche deposit of Nevado de Colima Volcano (Mexico). *J Volcanol Geoth Res* 117:213–235
- Capra L, Macías JL, Scott KM, Abrams M, Garduño-Monroy VH (2002) Debris avalanche and debris flow transformed from collapses in the Trans-Mexican Volcanic Belt, Mexico—behavior, and implication for hazard assessment. *J Vol Geotherm Res* 113:81110
- Capra L, Bernal JP, Carrasco-Núñez G, Roverato M (2013) Climatic fluctuations as a significant contributing factor for volcanic collapses. Evidence from Mexico during the Late Pleistocene. *Global Planet Change* 100:194–203
- Capra L, Roverato M, Bernal JP, Cortes A (2021) Evidence of the Early Holocene eruptive activity of Volcán de Colima and the 8.2 kyr global climatic event in lacustrine sediments from a debris avalanche-dammed lake. In: Di Capua, A., De Rosa, R., Kereszturi, G., Le Pera, E., Rosi, M. and Watt, S. F. L. (eds) *Volcanic processes in the sedimentary record: when volcanoes meet the environment*. Geological Society, London, Special Publications 520.
- Clavero JE, Sparks RSJ, Huppert HE (2002) Geological constraints on the emplacement mechanism of the Parinacota avalanche, northern Chile. *Bull Volcanol* 64:40–54
- Cortés A, Macías JL, Capra L, Garduño-Monroy VH (2010) Sector collapse of the SW flank of Volcán de Colima, México. The 3600 yr BP La Lumbre-Los Ganchos debris avalanche and associated debris flows. *J Volcanol Geoth Res* 189:52–66
- Cortés A, Komorowski JC, Macías JL, Capra L, Layer PW (2019) Late Pleistocene-Holocene debris avalanche deposits from Volcán de Colima, Mexico. In: Varley N, Connor C, Komorowski JC. (eds) *Volcán de Colima. Active volcanoes of the world*. Springer, Berlin, Heidelberg. https://doi.org/10.1007/978-3-642-25911-1_4
- Davies TR, McSaveney MJ (2009) The role of rock fragmentation in the motion of large landslides. *Eng Geol* 109:67–79
- Dufresne A, Zernack A, Bernard K, Thouret JC, Roverato M (2021) Sedimentology of volcanic Debris avalanche deposits. In: Roverato M, Dufresne A, Procter J (eds) *Volcanic debris avalanches: from collapse to hazard, advances in volcanology*. Springer book series advances in volcanology 364
- Folk RL, Ward WC (1957) Brazos River bar: a study in the significance of grain size parameters. *J Sediment Petrol* 27:3–26
- Le Friant A, Heinrich P, Deplus C, Boudon G (2003) Numerical simulation of the last flank-collapse event of Montagne Pelee, Martinique, Lesser Antilles. *Geophys Res Lett* 30(2) <https://doi.org/10.1029/2002GL015903>
- Glicken H (1996) Rockslide-debris avalanche of May 18, 1980, Mount St Helens volcano, Washington: U.S. Geological Survey Open-file Report 96-677, p 90
- Gómez-Tuena A, Orozco-Esquivel MT, Ferrari L (2007) Igneous petrogenesis of the Trans-Mexican Volcanic Belt. *Geol Soc Am Spec Pap* 422:129–181
- Kelfoun K, Druit TH (2005) Numerical modeling of the emplacement Socompa rock avalanche. Chile. *J Geoph Res* 110:B12202. <https://doi.org/10.1029/2005JB003758>
- Komorowski JC, Glicken H, Sheridan MF (1991) Secondary electron imagery of microcracks and hackly fractures in sand-size clasts from the 1980 Mount St. Helens debris-avalanche deposits, implications for particle-particle interactions. *Geology* 19:261–264
- Komorowski JC, Navarro C, Cortés A, Saucedo R, Gavilanes JC, Siebe C, Espíndola JM, Rodríguez-Elizarrarás SR, 1997, The Colima volcanic complex: International Association of Volcanology and Chemistry of the Earth's Interior (IAVCEI) General Assembly, Puerto Vallarta, México, Field Guide 3.

- Luhr JF, Prestegard KL (1988) Caldera formation at Volcan the Colima, Mexico, by a large Holocene volcanic debris avalanche. *J Volcanol Geoth Res* 35:335–348
- Makris S, Manzella I, Cole P, Roverato M (2020) Grain size distribution and sedimentology in volcanic mass-wasting flows: implications for propagation and mobility. *Int J Earth Sci.* <https://doi.org/10.1007/s00531-020-01907-8>
- Makris S, Roverato M, Dávila-Harris P, Cole P, Manzella I (2023a) Distributed stress fluidisation: insights into the propagation mechanisms of the Abona volcanic debris avalanche (Tenerife) through a novel method for indurated deposit sedimentological analysis. *Front Earth Sci* 11:1177507
- Makris S, Roverato M, Lomoschitz A, Cole P, Manzella I (2023b) The propagation and emplacement mechanisms of the Tenteniguada volcanic debris avalanche (Gran Canaria): field evidence for brittle fault-accommodated spreading. *J Volcanol Geotherm Res* 435:107773
- Neglia F, Sulpizio R, Dioguardi F, Capra L, Sarocchi D (2021) Shallow-water models for volcanic granular flows: a review of strengths and weaknesses of TITAN2D and FLO2D numerical codes. *J Volcanol Geoth Res* 410:107146
- Norini G, Capra L, Groppelli G, Agliardi F, Pola A, Cortés A (2010) The structural architecture of the Colima volcanic complex. *J Geophys Res Solid Earth* 115:B12209
- Norini G, Bustos E, Arnoso M, Zuluaga MC, Roverato M (2020) Unusual volcanic instability and sector collapse configuration at Chimpa volcano, central Andes. *J Volcanol Geoth Res* 393:106807
- Paguican EM, Roverato M, Yoshida H (2021) Volcanic debris avalanche transport and emplacement mechanisms. In: Roverato, M., Dufresne, A., Procter, J. (Eds.), *Volcanic debris avalanches: from collapse to hazard*. Springer book series advances in volcanology 364.
- Paguican EM, van Wyk de Vries B, Lagmay AMFA, (2014) Hummocks: how they form and how they evolve in rockslide-debris avalanches. *Landslides* 11:67–80
- Palmer BA, Alloway BV, Neall VE (1991) Volcanic debris avalanche deposits in New Zealand - lithofacies organization in unconfined, wet avalanche flows, en Fisher R.V., Smith G.A., (ed.), *Sedimentation in volcanic settings: Tulsa, Oklahoma, USA, Society for Sedimentary Geology, SEPM Special Publication* 45:89–98.
- Pardo M, Suarez G (1993) Steep subduction geometry of the Rivera plate beneath the Jalisco block in western Mexico. *Geophys Res Lett* 20:2391–2394
- Patra AK, Bauer AC, Nichita C, Pitman EB, Sheridan MF, Bursik M (2005) Parallel adaptive numerical simulation of dry avalanches over natural terrain. *J Volcanol Geoth Res* 139:1–2
- Patra A, Bevilacqua A, Akhavan-Safaei A, Pitman EB, Bursik M, Hyman D (2020) Comparative analysis of the structures and outcomes of geophysical flow models and modeling assumptions using uncertainty quantification. *Front Earth Sci* 8:275
- Perinotto H, Schneider JL, Bachelery P, Le Bourdonnec FX, Famin V, Michon L (2015) The extreme mobility of debris avalanches: a new model of transport mechanism. *J Geophys Res Solid Earth* 120(12):8110–9
- Pitman EB, Le L (2005) A two-fluid model for avalanche and debris flows. *Philos Trans Royal Soc a: Mathematical, Phys Eng Sci* 363:1471–2962
- Ponce L, Gaulon R, Suárez G, Lomas E (1992) Geometry and state of stress of the downgoing Cocos plate in the Isthmus of Tehuantepec, Mexico. *Geophys Res Lett* 19:773–776
- Procter J, Cronin S, Zernack A (2021) Computer simulation of a volcanic debris avalanche: a from Mt. Taranaki. In: Roverato M, Dufresne A, Procter J (eds) *Volcanic debris avalanches: from collapse to hazard*. Springer book series advances in volcanology 364
- Robin C, Mossand P, Camus G, Cantagrel JM, Gourgaud A, Vincent PM (1987) Eruptive history of the Colima volcanic complex (Mexico). *J Volcano Geotherm Res* 31:99–113
- Roverato M (2016) The Montesbelos mass-flow (southern Amazonian craton, Brazil): a Paleoproterozoic volcanic debris avalanche deposit? *Bull Volcanol* 78:49
- Roverato M, Capra L (2013) Características microtexturales como indicadores del transporte y emplazamiento de dos depositos de avalancha de escombros del Volcan de Colima (Mexico). *Revista Mexicana De Ciencias Geológicas* 30:512–525
- Roverato M, Capra L, Sulpizio R, Norini G (2011) Stratigraphic reconstruction of two debris avalanche deposits at Colima volcano (Mexico): insights into pre-failure conditions and climate influence. *J Volcanol Geotherm Res* 207:33–46
- Roverato M, Capra L, Sulpizio R (2013) First evidence of hydromagmatism at Colima volcano (Mexico). *J Volc Geoth Res* 249:197–200
- Roverato M, Cronin S, Procter J, Capra L (2015) Textural features as indicators of debris avalanche transport and emplacement, Taranaki volcano. *Bull Geol Soc Am* 127:3–18
- Roverato M, Larrea P, Casado I, Mulas M, Béjar G, Bowman L (2018) Characterization of the Cubilche debris avalanche deposit, a controversial case from the northern Andes, Ecuador. *J Volcanol Geotherm Res* 360:22–35
- Roverato M, Di Traglia F, Procter J, Paguican EM, Dufresne A (2021) Factors contributing to volcano lateral collapse. In: Roverato M, Dufresne A, Procter J (eds) *Volcanic debris avalanches: from collapse to hazard*. Springer book series advances in volcanology 364
- Siebert L, Glicken H, Ui T (1987) Volcanic hazard from Bezymianny and Bandai type eruption. *Bull Volcanol* 49:435–459
- Siebert L, Kimberly P, Pullinger CR (2004) The voluminous Acajutla debris avalanche from Santa Ana volcano, western El Salvador, and comparison with other Central American edifice-failure events. *Geol Soc Am Spec Pap* 375:5–24
- Sosio R, Crosta GB, Hungr O (2012) Numerical modeling of debris avalanche propagation from collapse of volcanic edifices. *Landslides* 9:315–334
- Stoopes GR, Sheridan MF (1992) Giant debris avalanches from the Colima volcanic complex, Mexico, implication for long runout landslides (>100 km). *Geology* 20:299–302
- Trofimovs J, Cas RAF, Davis BK (2004) An Archean submarine volcanic debris avalanche deposit, Yilgarn Craton, western Australia, with komatiite, basalt and dacite megablocks: the product of dome collapse. *J Volcanol Geotherm Res* 138:111–126
- Zernack AV, Cronin SJ, Neall VE, Procter JN (2010) A medial to distal volcanoclastic record of an andesite stratovolcano: detailed stratigraphy of the ring-plain succession of southwest Taranaki. *New Zealand: International Journal of Earth Sciences (geologische Rundschau)* 100:1937–1966

Supplementary Information The online version contains supplementary material available at <https://doi.org/10.1007/s10346-024-02335-4>.

Matteo Roverato (✉)

BIGEA, Alma Mater Studiorum, Università Di Bologna, Bologna, Italy
Email: matteo.roverato@unibo.it

Lucia Capra

Instituto de Geociencias, Universidad Nacional Autonoma de Mexico, Juriquilla, Queretato, Mexico